RMetS
Royal Meteorological Society

Assessing implicit large eddy simulation for two-dimensional flow

James Kent,[ab]* John Thuburn[a] and Nigel Wood[c]†

[a]*Mathematics Research Institute, College of Engineering, Mathematics and Physical Sciences, University of Exeter, UK*
[b]*Department of Atmospheric, Oceanic and Space Sciences, University of Michigan, Ann Arbor, Michigan, USA*
[c]*Met Office, Exeter, UK*

*Correspondence to: J. Kent, Department of Atmospheric, Oceanic and Space Sciences, University of Michigan, 2455 Hayward St, Ann Arbor, MI 48109-2143, USA. E-mail: jdkent@umich.edu
†The contribution of these authors was written in the course of their employment at the Met Office, UK, and is published with the permission of the Controller of HMSO and the Queen's Printer for Scotland

Numerical models of the atmosphere cannot resolve all relevant scales; the effects of unresolved scales on resolved scales must be represented by a subgrid model or parametrization. When the unresolved scales are similar in character to the resolved scales (as in three-dimensional or layerwise two-dimensional turbulence) the problem is essentially one of large eddy simulation. In this situation, one approach to subgrid modelling is implicit large eddy simulation (ILES), where the truncation errors of the numerical model attempt to act as the subgrid model. ILES has been shown to have some success for three-dimensional turbulence, but the validity of the approach has not previously been examined for two-dimensional or layerwise two-dimensional flow, which is the regime relevant to weather and climate modelling. Two-dimensional turbulence differs qualitatively from three-dimensional turbulence in several ways, most notably in having upscale energy and downscale enstrophy transfers. The question is of practical importance since many atmospheric models in effect use the ILES approach, for example through the use of a semi-Lagrangian advection scheme. In this paper a number of candidate numerical schemes are tested to determine whether their truncation errors can approximate the subgrid terms of the barotropic vorticity equation. Results show that some schemes can implicitly model the effects of the subgrid term associated with the stretching and thinning of vorticity filaments to unresolvable scales; the subgrid term is then diffusive and is associated with the downscale enstrophy transfer. Conservation of vorticity, by using a flux form scheme rather than advective form for advection of vorticity, was found to improve performance of a candidate ILES scheme. Some effects of the subgrid terms could not be captured by any of the schemes tested, whether using an implicit or a simple explicit subgrid model: none of the schemes tested is able to capture the upscale transfer of energy from unresolved to resolved scales. Copyright © 2011 Royal Meteorological Society and British Crown Copyright, the Met Office

Key Words: turbulence models; finite volume methods; incompressible flow; turbulent flow; cascade; MILES

Received 8 April 2011; Revised 25 July 2011; Accepted 11 August 2011; Published online in Wiley Online Library 14 September 2011

Citation: Kent J, Thuburn J, Wood N. 2012. Assessing implicit large eddy simulation for two-dimensional flow. *Q. J. R. Meteorol. Soc.* **138**: 365–376. DOI:10.1002/qj.925

1. Introduction

Atmospheric flow involves an enormous range of spatial scales. Numerical models of the atmosphere cannot in general resolve all relevant scales, so the effects of unresolved scales on resolved scales must be represented by a subgrid model or parametrization. When the unresolved processes are qualitatively different in character from the resolved processes, for example unresolved convection or gravity wave drag, then specific, process-based parametrizations must be used. On the other hand, when the unresolved scales are essentially similar in character to the resolved scales, as in three-dimensional or layerwise two-dimensional turbulence, then the approach of large eddy simulation (LES) may be used. LES is a technique for turbulence modelling in which the flow fields are formally filtered to separate them into large-scale and subfilter-scale components. Since the filter scale is almost always chosen to be similar to the grid scale, these components are usually referred to as resolved and subgrid-scale respectively. The governing equations then comprise terms involving only resolved scales, which are approximated by a direct discretization, and terms expressing the effects of subgrid scales on the resolved scales, which are approximated by a subgrid model (see section 2). Implicit large eddy simulation (ILES) attempts to use the truncation error of the discretization to act as the subgrid model. If it works, ILES provides an elegant and economical solution to the problem of subgrid modelling, exploiting properties of the discretization developed for other reasons, such as upwinding or flux limiting. A benefit of ILES is that there are no explicit parameters that need to be tuned to the flow. There have been a number of studies of the validity of ILES for three-dimensional turbulence (Sagaut, 2001; Grinstein *et al.*, 2007b), and some success has been demonstrated. However, little attention has been paid to the two-dimensional case; in particular, there has been no detailed examination of whether the truncation errors of any scheme do indeed match the subgrid term.

The aim of this paper is to examine the validity of ILES for two-dimensional flow. Two-dimensional turbulence has qualitatively different dynamics from three-dimensional turbulence. It is therefore not clear whether the successes of ILES for three-dimensional flow will carry over to two-dimensional flow. For three-dimensional incompressible turbulence in neutral stratification, energy is an important conservable quantity; on average, energy cascades downscale from the large scales to the small scales. In contrast, two-dimensional incompressible flow has a material invariant, the (absolute) vorticity, implying an infinite family of conserved moments of vorticity, including the enstrophy. In two-dimensional turbulence the energy is transferred upscale and it is the enstrophy that cascades downscale. The upscale transfer of energy might make ILES less suitable for modelling two-dimensional turbulence; ILES tends to be less accurate for three-dimensional turbulence in situations with significant upscale energy transfer (backscatter), such as near walls (Brown *et al.*, 2000). On the other hand, the energy spectrum is much steeper in two-dimensional turbulence than in three-dimensional turbulence, suggesting a stronger slaving of small scales to large, which could make two-dimensional turbulence more amenable to the ILES approach.

The main motivation for this study is to understand, and if possible justify, the use of ILES-like schemes in numerical weather and climate models. Due to the effects of rotation and stratification, large-scale atmospheric flow can be considered analogous to two-dimensional flow: potential vorticity is a material invariant (analogous to the vorticity), potential enstrophy (analogous to the enstrophy) is one member of an infinite family of conserved quantities, and energy is transferred upscale while potential enstrophy cascades downscale. Two-dimensional turbulence is therefore an appropriate paradigm to consider.

An important element of the dynamical core of a numerical weather or climate model is the transport scheme. Different dynamical cores model the subgrid terms associated with nonlinear advection in different ways. Simple subgrid models of the form ∇^4 are common. So too is the use of semi-Lagrangian (SL) advection schemes without explicit subgrid models (Williamson, 2007); the diffusive nature of the interpolation is used to model the subgrid terms in much the same way that ILES works. There is growing interest in the use of finite-volume schemes using flux limiters or Riemann solvers (e.g. Lin, 2004; Ullrich *et al.*, 2010), which again are inherently dissipative.

Modified equation analysis can be used to show qualitative similarities between the truncation errors of some numerical schemes and the subgrid terms (e.g. Margolin and Rider, 2002, 2007, and references therein). However, both modified equation analysis and the method used to approximate the subgrid terms make use of Taylor series approximations. The convergence rate of Taylor series depends on the smoothness of the function being approximated. The flows of interest have rather shallow energy spectra and are not very smooth, implying that leading-term Taylor series approximations are not quantitatively accurate. We have confirmed this by direct calculation of the subgrid terms and their Taylor series approximations for several model problems. Therefore, in this paper we take a more direct approach to testing the validity of ILES (section 3). We develop a framework, using a coarse-resolution test solution together with a high-resolution reference solution and a high-resolution solution constructed to be free of the effects of scales that the coarse resolution cannot resolve, which allows the direct calculation of the cumulative effect of both the coarse-grid truncation error and the subgrid term, allowing the two to be compared. Similar approaches, though with important differences of detail, have been used for example by Berloff (2005) and Hermanson *et al.* (2009) to estimate the subgrid term in ocean and atmosphere models.

Previous work (Grinstein and Fureby, 2006) suggests that nonlinear diffusion, such as that associated with a flux limiter, is required for three-dimensional ILES. It is important to determine whether this is also true for two-dimensional ILES. Therefore in this paper schemes with both linear and nonlinear diffusion are tested on the barotropic vorticity equation. It has also been suggested (e.g. Margolin and Rider, 2002) that for three-dimensional ILES the flux form (the conservative form) of the numerical scheme is required to produce satisfactory results. Here numerical schemes in both flux and advective forms are tested to determine whether conservation is important for two-dimensional ILES, and whether conservation of momentum or vorticity is more important. The governing equations along with the numerical schemes used in this paper are discussed in section 2. Section 3 describes the methodology

used for the numerical testing and calculation of the subgrid term. Results are found in section 4 and conclusions are drawn in section 5.

2. Basic equations and numerical schemes

The inviscid barotropic vorticity equation (BVE) in Cartesian coordinates is

$$\frac{\partial \zeta}{\partial t} + u\frac{\partial \zeta}{\partial x} + v\frac{\partial \zeta}{\partial y} = 0, \tag{1}$$

in advective form and

$$\frac{\partial \zeta}{\partial t} + \frac{\partial u\zeta}{\partial x} + \frac{\partial v\zeta}{\partial y} = 0, \tag{2}$$

in flux form, where $\zeta = \partial v/\partial x - \partial u/\partial y$ is the vorticity and u and v are the velocity components in the x and y directions respectively. The flow is incompressible:

$$\frac{\partial u}{\partial x} + \frac{\partial v}{\partial y} = 0, \tag{3}$$

and therefore (1) and (2) are equivalent. The velocity can be calculated from ζ via the stream function ψ:

$$\nabla^2 \psi = \zeta, \tag{4}$$

$$u = -\frac{\partial \psi}{\partial y}, \tag{5}$$

$$v = \frac{\partial \psi}{\partial x}. \tag{6}$$

In this paper the domain used is doubly periodic (of size 1) and all units are dimensionless.

Numerical testing will also take place using the velocity form of the two-dimensional Euler equations and the two-dimensional quasi-geostrophic potential vorticity equation. Although the continuous velocity form of the Euler equations and the continuous BVE are equivalent, the filtered forms and discretizations are not. We examine both the BVE and the Euler equations to determine whether one or other form is more suitable for the use of ILES. The velocity form of the Euler equations is

$$\frac{\partial u}{\partial t} + \frac{\partial uu}{\partial x} + \frac{\partial vu}{\partial y} + \frac{\partial P}{\partial x} = 0, \tag{7}$$

$$\frac{\partial v}{\partial t} + \frac{\partial uv}{\partial x} + \frac{\partial vv}{\partial y} + \frac{\partial P}{\partial y} = 0, \tag{8}$$

where P is pressure divided by density (and density is constant). A diagnostic equation is solved for P to ensure incompressibility.

The quasi-geostrophic potential vorticity equation has the same form as the BVE:

$$\frac{\partial q}{\partial t} + \frac{\partial uq}{\partial x} + \frac{\partial vq}{\partial y} = 0, \tag{9}$$

but the stream function is calculated as

$$\nabla^2 \psi - \frac{\psi}{\lambda^2} = q, \tag{10}$$

where q is the potential vorticity and λ is the Rossby radius (see Gill, 1982, for a full derivation). The influence of a point vortex falls off exponentially beyond the Rossby radius, so that vortex interactions are weaker than for the BVE, which corresponds to the case of infinite Rossby radius. The BVE is used as an idealized problem, whereas the quasi-geostrophic potential vorticity equation is more relevant to the application to atmospheric modelling due to the finite Rossby radius. Because vortex interactions, and hence energy and (potential) enstrophy transfers, are sensitive to the Rossby radius, the conclusions concerning ILES are potentially sensitive to the Rossby radius too.

2.1. Subgrid analysis

A filter is used to separate the large scales (denoted by an overbar) and small scales (denoted by a prime). Filtered equations are usually written by replacing each field in the original equation with its filtered version, and then introducing a compensating subgrid term on the right-hand side. For example, the filtered BVE becomes

$$\frac{\partial \bar{\zeta}}{\partial t} + \frac{\partial \bar{u}\bar{\zeta}}{\partial x} + \frac{\partial \bar{v}\bar{\zeta}}{\partial y} = \mathrm{SG}, \tag{11}$$

where SG denotes the subgrid term

$$\mathrm{SG} = \frac{\partial}{\partial x}\left(\bar{u}\bar{\zeta} - \overline{u\zeta}\right) + \frac{\partial}{\partial y}\left(\bar{v}\bar{\zeta} - \overline{v\zeta}\right). \tag{12}$$

(Under suitable approximations, e.g. Reynolds averaging for which $\bar{\bar{a}} = \bar{a}$ and $\overline{a\bar{b}} = \bar{a}\bar{b}$,

$$\mathrm{SG} \approx -\frac{\partial}{\partial x}\left(\overline{u'\zeta'}\right) - \frac{\partial}{\partial y}\left(\overline{v'\zeta'}\right), \tag{13}$$

but we will not make use of this.) The incompressibility condition becomes

$$\frac{\partial \bar{u}}{\partial x} + \frac{\partial \bar{v}}{\partial y} = 0. \tag{14}$$

2.2. Definition of subgrid term

For the methodology described in section 3 it is desirable to calculate a solution without the effects of the subgrid term. An obvious attempt would be to solve an equation analogous to (11) with SG set to zero:

$$\frac{\partial \zeta^S}{\partial t} + \frac{\partial u^S\zeta^S}{\partial x} + \frac{\partial v^S\zeta^S}{\partial y} = 0. \tag{15}$$

The intention here is that ζ^S should be a smooth vorticity field, with u^S and v^S the corresponding velocities. However, (15) is simply the original unfiltered BVE (1) with a change of notation; thus, even if ζ^S is initially smooth, the nonlinear terms will inevitably generate small scales, and the resulting solution will not remain free of the effects of the subgrid term.

To use our methodology we require a modified definition of the subgrid terms:

$$\frac{\partial \bar{\zeta}}{\partial t} + \overline{\frac{\partial \bar{u}\bar{\zeta}}{\partial x}} + \overline{\frac{\partial \bar{v}\bar{\zeta}}{\partial y}} = \mathrm{SG}^*, \tag{16}$$

where

$$\mathrm{SG}^* = \frac{\partial}{\partial x}\left(\overline{\bar{u}\bar{\zeta}} - \overline{u\zeta}\right) + \frac{\partial}{\partial y}\left(\overline{\bar{v}\bar{\zeta}} - \overline{v\zeta}\right). \qquad (17)$$

(Note there is no approximation here, just a redefinition of the subgrid term. A similar decomposition is discussed by Leonard, 1975, and Sagaut, 2001). Now a smooth solution can be defined by solving an equation analogous to (16) with SG* set to zero:

$$\frac{\partial \zeta^S}{\partial t} + \frac{\partial \overline{u^S\zeta^S}}{\partial x} + \frac{\partial \overline{v^S\zeta^S}}{\partial y} = 0. \qquad (18)$$

Provided ζ^S is initially smooth, all terms in (18) are smooth, so ζ^S evolves without the influence of subgrid terms, as required.

Although less familiar, the form (16), (17) provides a cleaner separation of the governing equations into resolved scale and subgrid scale components than (11), (12) (Sagaut, 2001) and so may be useful in other contexts too. In particular, both sides of (16) are smooth. The conditions required for ILES to be successful can be used to relate the form (16), (17) to Sagaut's decomposition (Sagaut, 2007) of numerical model errors into projection errors, discretization errors, and resolution errors (see Appendix). The two forms of the subgrid term are related by

$$\mathrm{SG}^* - \overline{\mathrm{SG}} = \frac{\partial}{\partial x}\left(\overline{\overline{u\zeta}} - \overline{u\zeta}\right) + \frac{\partial}{\partial y}\left(\overline{\overline{v\zeta}} - \overline{v\zeta}\right). \qquad (19)$$

For the cell average filter (see section 2.3) that will be used for the numerical testing, $\overline{\overline{(.)}} \neq \overline{(.)}$, so SG* is not simply a filtered version of SG.

2.3. Cell average filter

Throughout this paper the cell average filter will be used. The filter is defined by

$$\overline{u}(x,y) = \frac{1}{\Delta x}\frac{1}{\Delta y}\int_{x-\frac{\Delta x}{2}}^{x+\frac{\Delta x}{2}}\int_{y-\frac{\Delta y}{2}}^{y+\frac{\Delta y}{2}} u(\tilde{x},\tilde{y})\,\mathrm{d}\tilde{y}\,\mathrm{d}\tilde{x}, \qquad (20)$$

where Δx and Δy are the width of the filter in the x and y directions respectively and $\tilde{x}$ and $\tilde{y}$ are dummy variables. (In the numerical tests Δx and Δy are the coarse-resolution (CR) grid spacings, making the filter scale the same size as a CR cell, and the integrals are approximated by discrete sums.) This is a natural filter for finite-volume schemes because a sample of a filtered field at a point corresponds to a cell average of the original field; it is commonly used in LES (Grinstein *et al.*, 2007b).

2.4. Numerical schemes

A number of numerical schemes will be considered to determine how well they implicitly capture the subgrid term of the barotropic vorticity equation through their truncation error. A 'Benchmark' scheme, composed of a second-order accurate scheme with a simple subgrid model, will be used to compare the accuracy of implicit subgrid models with a simple explicit subgrid model. For ILES to be useful for two-dimensional flow, the candidate ILES numerical scheme must be no worse than the Benchmark scheme, i.e. the implicit subgrid model of the ILES schemes must be at least as accurate as a simple explicit subgrid model. The Benchmark scheme will use the energy- and enstrophy-conserving Arakawa Jacobian (Arakawa, 1966) with a subgrid model of the form $\kappa\nabla^4\zeta$. Here κ is a constant that is tuned to ensure that the solution is neither overdiffused nor noisy at the grid scale; for this paper $\kappa = -0.2\Delta_C^4$, where Δ_C is the grid spacing of the CR grid, unless stated otherwise. (The need for such flow-dependent tuning is a significant and well-known disadvantage of linear hyperviscosity models–see, for example, Jablonowski and Williamson, 2011.)

It has been suggested that ILES should be successful for three-dimensional flow when the truncation error is diffusive and second order in the grid spacing (Grinstein *et al.*, 2007a), as the subgrid terms can be shown, using Taylor series approximation, to be diffusive and second order. The Lax–Wendroff scheme with the van Leer flux limiter (van Leer, 1974) is second-order accurate, but when the flux limiter is zero it has a diffusive truncation error, and therefore should be a suitable candidate scheme for ILES. For this reason we include it among the schemes tested.

Although the continuous equations (1) and (2) are equivalent, discretizations of them are generally not. It has been suggested that the flux form of the numerical scheme, guaranteeing conservation of the predicted variable, is essential to the success of ILES for three-dimensional flow (Margolin and Rider 2002). To test this idea for two-dimensional flow the Lax–Wendroff Flux Limiter scheme in both flux form (i.e. a discretization of (2)) and advective form (a discretization of (1)) will be used.

It has been suggested (Grinstein and Fureby, 2006) that some form of nonlinear diffusion is required for ILES to work accurately for three-dimensional turbulence modelling, and this can be achieved by using a flux limiter. To test whether nonlinear diffusion is required for two-dimensional ILES a scheme that contains linear diffusion will be tested with and without the addition of a flux limiter. The Utopia scheme (Leonard *et al.*, 1993) is a third-order scheme, for linear advection, that has a diffusive truncation error. A flux limiter can easily be applied (Thuburn, 1996). These two schemes–Utopia and Utopia with a flux limiter–can be compared to determine whether there is a significant improvement in using the flux limiter and therefore whether a flux limiter, or some sort of nonlinear diffusion, is beneficial for two-dimensional ILES.

Semi-Lagrangian (SL) schemes (Staniforth and Côté, 1991) are often used in atmospheric models because a larger time step can be used than with Eulerian methods. Using bi-cubic Lagrange interpolation, the SL scheme is third-order accurate for linear advection, similar to the Utopia scheme; however, the SL scheme that we use does not conserve the advected quantity. (Note that this is in contrast to some types of SL schemes which are conservative; see, for example, Zerroukat *et al.*, 2002, and Lauritzen *et al.*, 2010.) Comparing our SL scheme with the Utopia scheme will provide another comparison between conservative and non-conservative schemes that are otherwise similar, as well as testing the ILES performance of a scheme that is of great practical relevance in weather and climate modelling.

The Arakawa Jacobian (Arakawa, 1966) will also be tested without the subgrid model. This scheme is dispersive and has no theoretical motivation to be successful for ILES. However,

comparing the Arakawa Jacobian with the 'suitable' ILES schemes will show how much of an improvement (if any) the ILES schemes can make.

Table I summarizes the numerical schemes that will be tested for the barotropic vorticity equation. The third column indicates the formal order of accuracy of the numerical scheme for linear advection, and the fourth column indicates whether the scheme conserves the advected quantity.

All of the numerical schemes will be used with a red/black multigrid elliptic solver (Fulton *et al.*, 1986) to calculate the stream function.

The same numerical schemes shown in Table I will be used for the quasi-geostrophic potential vorticity equation. The Lax–Wendroff scheme with the van Leer limiter and the Utopia schemes will be used for the momentum form of the Euler equations. The red/black multigrid elliptic solver will be used to calculate the pressure.

3. Methodology

For some chosen initial condition, a high-resolution (HR) reference solution, denoted by ζ^H, is calculated on a grid with 2048 grid points in each spatial direction; the scheme used is the energy- and enstrophy-conserving Arakawa Jacobian with scale selective dissipation of the form $\kappa\nabla^4$ ($\kappa = -0.2\Delta_H^4$, where Δ_H is the grid spacing of the HR grid). Using an HR grid ensures that the reference solution is accurate on the scales of interest, at least for some time. (For example, comparing our HR solution with an even higher-resolution solution using a 4096^2 grid gives a normalized l_2 vorticity error norm of less than 0.008 at time 14.6 for the vortex merger test case, described in section 4.1 below.) The candidate numerical schemes described in section 2.4 are then used to integrate from the same initial condition on a number of different coarse-resolution (CR) grids. The HR solution explicitly resolves the subgrid scales, i.e. those scales finer than the resolution of the CR grid, whereas the CR grid solutions must attempt to capture the effects of the subgrid terms through their implicit or explicit subgrid models. Comparison of the HR and CR solutions indicates how well the candidate schemes achieve this. Moreover, comparison with a third, smooth solution allows the cumulative effects of the subgrid terms and truncation errors to be explicitly diagnosed and compared (see section 3.1).

To compare the accuracy of the numerical schemes the l_2 vorticity error is calculated as $|\overline{\zeta^H} - \zeta^C|_2$, where ζ^C indicates the solution generated by the candidate numerical scheme on the CR grid and the overbar represents filtering to the CR grid using averages over the coarse grid cells. If the truncation error of the CR numerical scheme is similar to the subgrid terms, then $\overline{\zeta^H} \approx \zeta^C$ and the l_2 error is small. If the truncation error of the CR numerical scheme is very different from the subgrid terms, then $\overline{\zeta^H}$ becomes very different from ζ^C and the l_2 error becomes large. The l_2 vorticity error is calculated at each time step, and the normalized l_2 error is used. The normalized l_2 error for vorticity plotted against time shows the accuracy of the numerical scheme as the solution evolves.

The downscale transfer of enstrophy from resolved to subgrid scales and the upscale transfer of energy from subgrid to resolved scales are mediated by the subgrid scales. An important test of an ILES scheme, therefore, is whether it can capture these transfers. For the continuous equations the energy is defined as

$$E = \frac{1}{2}\int u^2 + v^2 \mathrm{d}A, \tag{21}$$

where dA is the element of area and the integral is over the domain. This can be rewritten in terms of the stream function and simplified:

$$E = \frac{1}{2}\int \nabla\psi \cdot \nabla\psi \ \mathrm{d}A, \tag{22}$$

$$= \frac{1}{2}\int \nabla\cdot(\psi\nabla\psi) - \psi\nabla^2\psi \ \mathrm{d}A. \tag{23}$$

In a periodic domain $\int \nabla\cdot(\psi\nabla\psi)\,\mathrm{d}A = 0$; therefore

$$E = -\frac{1}{2}\int \psi\nabla^2\psi \ \mathrm{d}A, \tag{24}$$

$$= -\frac{1}{2}\int \psi\zeta \ \mathrm{d}A. \tag{25}$$

The energy contained in the HR reference solution at scales resolved by the CR grid is diagnosed:

$$E^H = -\frac{1}{2}\sum_k \overline{\psi^H}_k \overline{\zeta^H}_k \,\Delta x\,\Delta y, \tag{26}$$

and compared with the energy of the CR solution:

$$E^C = -\frac{1}{2}\sum_k \psi^C{}_k \zeta^C{}_k \,\Delta x\,\Delta y. \tag{27}$$

Here the sums are over the grid cells (index k) of the CR grid. Similarly, for enstrophy:

$$Z^H = \frac{1}{2}\sum_k \overline{\zeta^H}_k \overline{\zeta^H}_k \,\Delta x\,\Delta y, \tag{28}$$

$$Z^C = \frac{1}{2}\sum_k \zeta^C{}_k \zeta^C{}_k \,\Delta x\,\Delta y. \tag{29}$$

Time series of these diagnostics show how the energy and enstrophy on CR scales evolve for the reference and CR solutions.

3.1. *Numerical subgrid terms*

Numerically solving (18) produces a smooth solution ζ^S without the effects of the subgrid term. Computing ζ^S on the HR grid ensures that truncation errors are negligible and the scales of interest are captured accurately. The difference

$$\Delta_{\mathrm{SG}} = \overline{\zeta^H} - \zeta^S \tag{30}$$

therefore quantifies the cumulative effects of the subgrid term SG*. At the same time, the difference

$$\Delta_{\mathrm{TE}} = \zeta^C - \zeta^S \tag{31}$$

quantifies the cumulative effects of the truncation error in the CR solution (more precisely, the effects of the discretization error and projection error; see the Appendix). Therefore, comparison of Δ_{TE} and Δ_{SG} provides a direct measure of

Table I. List of schemes tested: the third column indicates the formal order of accuracy of the scheme for linear advection, and the fourth column shows whether the scheme is in conservative form.

Scheme	Leading error/SGM	Order	Conservative
Arakawa Jacobian	Dispersive, linear	2nd	Yes
Benchmark	∇^4, linear	2nd	Yes
LW van Leer (flux)	Diffusive, nonlinear	2nd	Yes
LW van Leer (advective)	Diffusive, nonlinear	2nd	No
Utopia	Diffusive, linear	3rd	Yes
Utopia 2D Limiter	Diffusive, nonlinear	3rd	Yes
Semi-Lagrangian	Diffusive, linear	3rd	No

how well the truncation error of the CR scheme captures the subgrid term.

(In this paper we concentrate on the cumulative effects of the subgrid term and truncation errors. It is also possible to diagnose the instantaneous subgrid term for a given vorticity field ζ^H and the instantaneous truncation error when this field is filtered to a CR grid and fed into a candidate ILES scheme. However, we have found that the results are then much more difficult to interpret. This appears to be because, when results from one scheme at one resolution are fed into another scheme at another resolution, there is an initial adjustment period during which the behaviour near the grid scale is rather different from the longer-term behaviour. This initial adjustment is discussed further in section 4.3.)

Conceptually, there are two types of behaviour that are represented by subgrid terms: Type (i) vorticity features being stretched and thinned by advection until their scale collapses below the CR grid scale; and Type (ii) subgrid features affecting the resolved scale vorticity, for example by wrapping up, by merging with each other, or by merging with the resolved scale features. These two types of behaviour can be seen in Figure 1, which shows the HR reference solution at time 14.6 for the vortex merger test case (described in section 4.1 below), and the cumulative effect of the subgrid terms Δ_{SG} calculated using the method specified above with a filter scale corresponding to a CR grid of 128 cells in each direction. The smaller vortex has been stretched out into a long vorticity tongue, and parts of it have been stretched below the CR grid scale. A section through the tongue shows a positive–negative–positive pattern in Δ_{SG}, indicating a diffusive broadening of the vorticity tongue (Type (i)). At the end of the vorticity tongue (near coordinates $(0.3, 0.3)$) Δ_{SG} shows a large positive–negative dipole; this is where the small vortex that has been stretched below the grid scale is merging with the large vortex (Type (ii)).

Another test case that demonstrates both types of subgrid behaviour is the vorticity strip test case. Here, a thin strip of vorticity is placed across the domain following a cosine pattern (described in section 4.1 below). The vorticity strip first stretches and then wraps up; the wrapping up creates larger-scale vorticity features. The HR solution and the cumulative effect of the subgrid terms (Δ_{SG} calculated with a filter scale corresponding to a CR grid of 128 cells in each direction), both at time 48.8, are shown in Figure 2. The plot of Δ_{SG} is zoomed into one of the wrapped-up vortices. A cross-section of the vorticity strip shows a positive–negative–positive pattern in Δ_{SG} where the strip has been stretched below the CR grid scale (Type (i)). In the centre of the wrapped-up vortex, Δ_{SG} shows positive values; this is where the stretched-out vorticity strip has wrapped up, regenerating a vorticity feature at the CR scale (Type (ii)).

4. Results

The numerical schemes are tested on a variety of different test cases. The vortex merger test case (see below) consists of two vortices such that one vortex is stretched out around the other, highlighting vorticity being stretched below the grid scale, before the stretched-out vortex merges with the other. The vorticity strip test case (see section 4.2) is designed so that an unstable strip of vorticity will be stretched out before wrapping itself up. These first two tests are idealized and show individual vortex interactions; they make up some of the 'building blocks' of turbulence. The freely decaying turbulence test (see section 4.3) is comprised of a domain full of already evolving vortices to test the ILES properties of the schemes in flows of realistic complexity.

As the first two tests are idealized, the vorticity pattern is predictable for the length of the simulation. For the freely decaying turbulence test the l_2 error norms are valid while the vorticity is predictable until time ~ 35 (this can be determined using convergence tests of the numerical schemes up to the HR grid). After this time it is only the total energy and enstrophy statistics that are measured.

4.1. *Vortex merger*

The vortex merger test case initializes a large vortex and a small vortex of the same sign in the domain. The large vortex (with peak 2 and radius 1/4) is centred at $(1/4, 1/2)$ and the small vortex (with peak 1 and radius 1/8) is centred at $(19/32, 1/2)$. The vortices are generated using cosine functions; if the distance from any point in the domain to the centre of the vortex is denoted d, the radius of the vortex is denoted r, and the peak of the vortex is denoted m, then the vorticity is initialized as

$$\zeta = \begin{cases} m \times \cos(\pi d/(2r))^2 & d \le r, \\ 0 & \text{otherwise.} \end{cases} \tag{32}$$

The global mean vorticity is subtracted from ζ to ensure that the global mean vorticity is zero for the initial conditions. The large vortex stretches out the small vortex. A time step of $\Delta t = 2^{-10}$ is used to ensure that the Courant number is less than 1 on the HR grid (and much less than 1 on the CR grids), so that the schemes are stable and the spatial errors dominate.

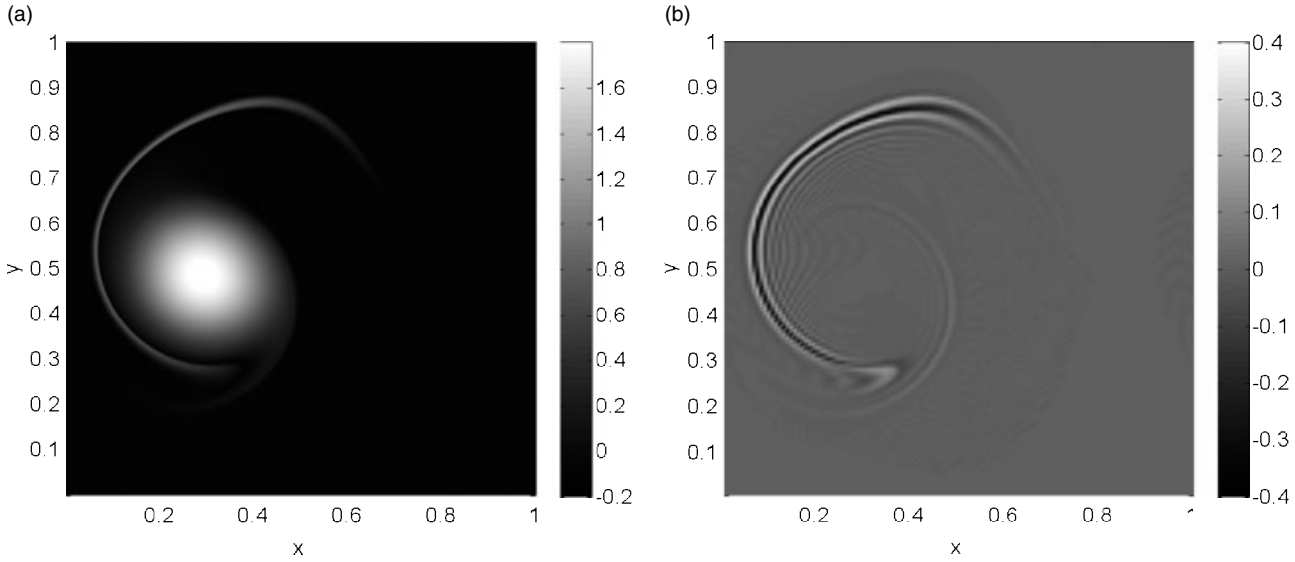

Figure 1. The high-resolution vorticity solution for the vortex merger test case at time 14.6 (a), and the cumulative effect of the subgrid terms, Δ_{SG}, on the 128^2 grid (b).

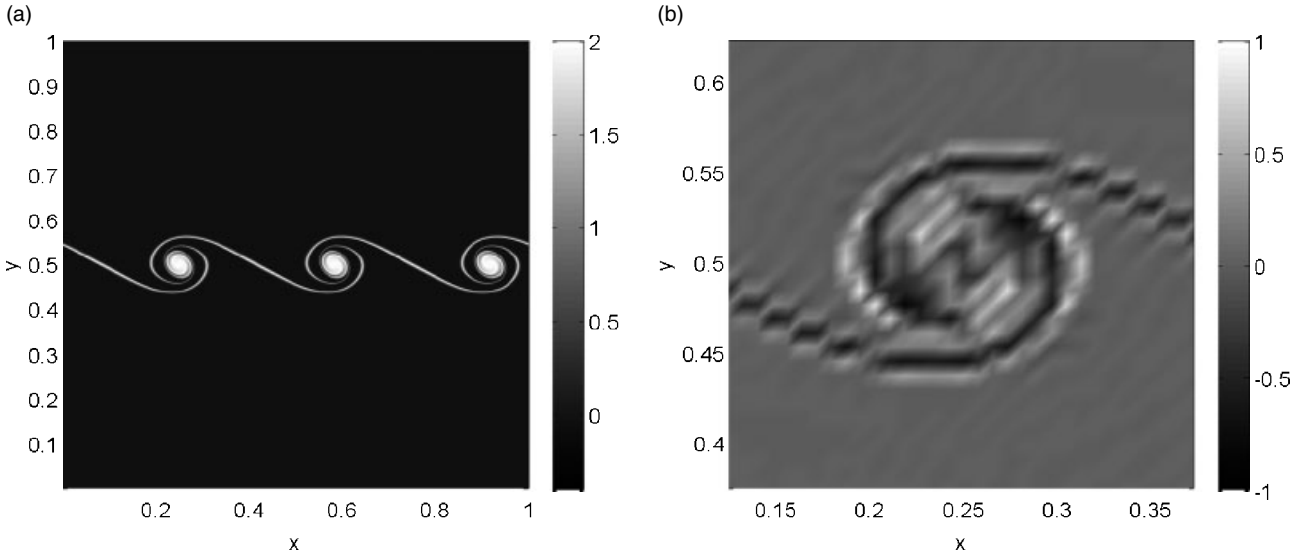

Figure 2. High-resolution reference solution for the vorticity strip test case at time 48.8 (a) and the cumulative effect of the subgrid terms, Δ_{SG}, on the 128^2 grid (b, zoomed in).

The cumulative truncation errors for the Arakawa Jacobian and Utopia schemes for the vortex merger test case at time 14.6 on the 128^2 grid are shown in Figure 3 (results at other resolutions are qualitatively similar). These plots can be compared with the right-hand plot of Figure 1. The Arakawa Jacobian's cumulative truncation error does not match the cumulative subgrid term; there are phase errors across the domain and the truncation error has a different sign from the subgrid term along the vorticity tongue remnant of the small vortex. Clearly the Arakawa Jacobian does not capture the subgrid term along the vorticity tongue. The actual subgrid term is diffusive (spreading features that are stretched below the grid scale) whereas the leading truncation error of the Arakawa Jacobian is dispersive. The Utopia scheme's truncation error is a good match to the subgrid term along the vorticity tongue, and this is because the leading order error of Utopia is diffusive. The magnitude of the Utopia scheme's truncation error is smaller than the magnitude of the subgrid terms (for example, the peak value is 15% smaller), indicating that the Utopia scheme does not capture all of the subgrid term. The normalized l_2 vorticity error norms for the vortex merger test case at time 14.6 on the 128^2 grid are 0.2099 for the Arakawa Jacobian and 0.0976 for the Utopia scheme.

For this test case the truncation errors for the Benchmark, Lax–Wendroff flux limiter (in both advective and flux forms), Utopia with the flux limiter and SL schemes are all very similar to that of the Utopia scheme, although the features of the truncation error of the Benchmark and Lax–Wendroff flux limiter schemes are more spread out than the Utopia scheme, implying excessive diffusion.

None of the schemes tested is able to capture the subgrid term feature near $(0.3, 0.3)$ where the stretched-out small vortex merges with the large vortex. The results for the vortex merger test case show that the candidate ILES schemes, and schemes with simple subgrid models, are able to capture the diffusive effect of the subgrid term as vorticity features are stretched beyond the grid scale, but are unable to model

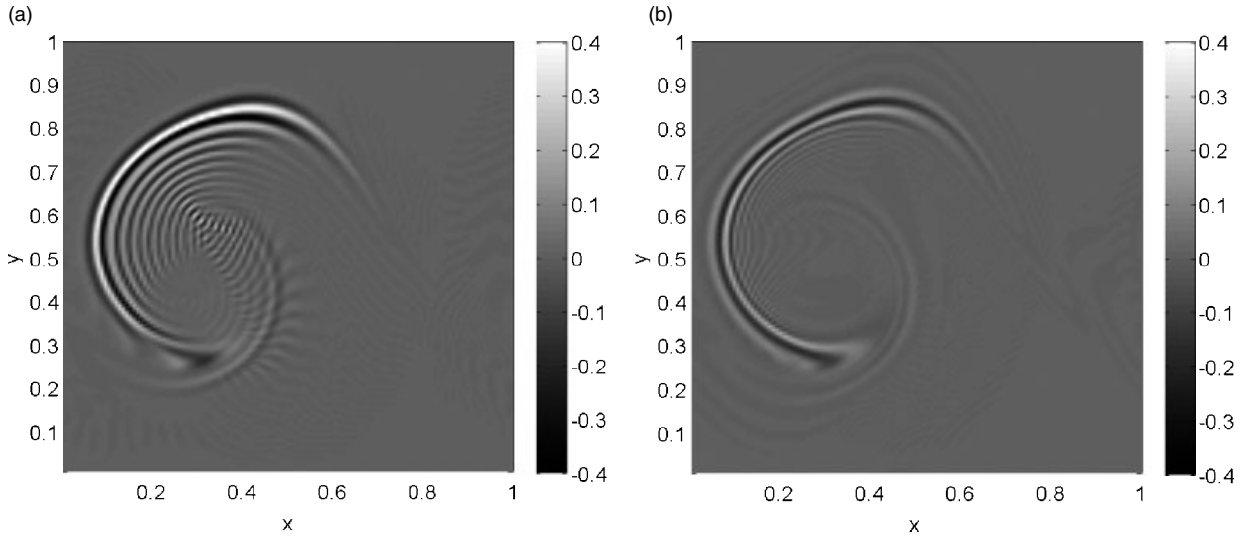

Figure 3. The cumulative truncation error for the Arakawa Jacobian (a) and the Utopia scheme (b) for the vortex merger test case at time 14.6 and on the 128^2 grid.

the effects of the subgrid term when subgrid-scale vorticity features are merging. The l_2 vorticity error norms indicate that the schemes considered for ILES have a comparable error norm to the Benchmark scheme, for each CR grid. These error norms are significantly smaller than the Arakawa Jacobian's error norm.

4.2. *Vorticity strip*

The numerical schemes are also tested on the vorticity strip test case. A strip of vorticity (with width 1/32 and magnitude 2) is placed across the domain following a $\cos(6\pi x)$ pattern. The centre of the strip lies along $y = 1/2 + 0.025\cos(6\pi x)$. The strip is created using cosine functions. For any point in the domain, (x_p, y_p), let $d = |y_p - (1/2 + 0.025\cos(6\pi x_p))|$; then the vorticity is initialized as

$$\zeta = \begin{cases} 2 \times \cos(\pi d/(2r))^2 & d \le r, \\ 0 & \text{otherwise}, \end{cases} \tag{33}$$

where $r = 1/64$. As with the vortex merger test case, the global mean vorticity is subtracted from ζ to ensure that the global mean vorticity is zero. The coefficient for the subgrid model of the Benchmark scheme is tuned to $\kappa = -0.05\Delta_C^4$; using larger values of κ results in the Benchmark scheme being too diffusive.

Figure 4 shows the cumulative truncation errors for the Benchmark scheme and the Utopia scheme with the flux limiter for the vorticity strip test case at time 48.8 on the 128^2 grid, zoomed into a wrapped-up vortex (again, results at other resolutions are qualitatively similar). These plots can be compared with the right-hand plot of Figure 2. The cumulative truncation errors for the Benchmark scheme and the Utopia flux limiter scheme both have a positive–negative–positive pattern across the strip; this is similar to the pattern of the cumulative subgrid term associated with the stretching of the strip. However, neither the Benchmark scheme nor the Utopia flux limiter scheme can properly re-create the positive pattern in the centre of the wrapped-up vortices. This reflects the fact that the numerical schemes on the CR grid cannot rebuild a resolved scale vorticity feature from vorticity features that have become subgrid scale (i.e. diffused out, from the point of view of the CR grid). The cumulative truncation error of the Benchmark scheme has large positive parts as the stretched-out vorticity approaches the wrapped-up vortex. This is due to the scale-selective dissipation being too diffusive. Note, however, that a smaller coefficient κ results in grid scale noise as the strip is stretched out. The cumulative truncation error of the Utopia scheme with the flux limiter has positive parts in the centre of the wrapped-up vortex, but this does not correspond to the positive parts in the effects of the subgrid terms; the Utopia scheme with the flux limiter cannot wrap up the vorticity strip that it has diffused. The normalized l_2 vorticity error norms for the vorticity strip test case at time 48.8 on the 128^2 grid are 0.832 for the Benchmark scheme, and 0.652 for the Utopia scheme with the flux limiter.

The truncation errors of the Lax–Wendroff flux limiter (in both advective and flux forms), Utopia and the SL schemes are all very similar to that of the Utopia scheme with the flux limiter; they capture the subgrid terms as the strip is stretched below the grid scale, but they cannot capture the subgrid terms as the strip wraps up. The Arakawa Jacobian (with no subgrid model) creates grid-scale noise as the strip is stretched out; this is due to the leading truncation error of the Arakawa Jacobian being dispersive.

4.3. *Freely decaying turbulence*

The first two test cases looked at highly idealized situations, allowing us to focus on specific features of the flow. In the third test case, the initial conditions are derived by allowing a field of vortices to freely evolve, generating a complex, fully turbulent vorticity field with structures at a range of scales. This evolved vorticity field is then used as the initial conditions for the freely decaying turbulence test case. The vorticity field given by

$$\begin{aligned} \zeta = {} & \sin(8\pi x)\sin(8\pi y) \\ & + 0.4\cos(6\pi x)\cos(6\pi y) \\ & + 0.3\cos(10\pi x)\cos(4\pi y) \\ & + 0.02\sin(2\pi y) + 0.02\sin(2\pi x), \end{aligned}$$

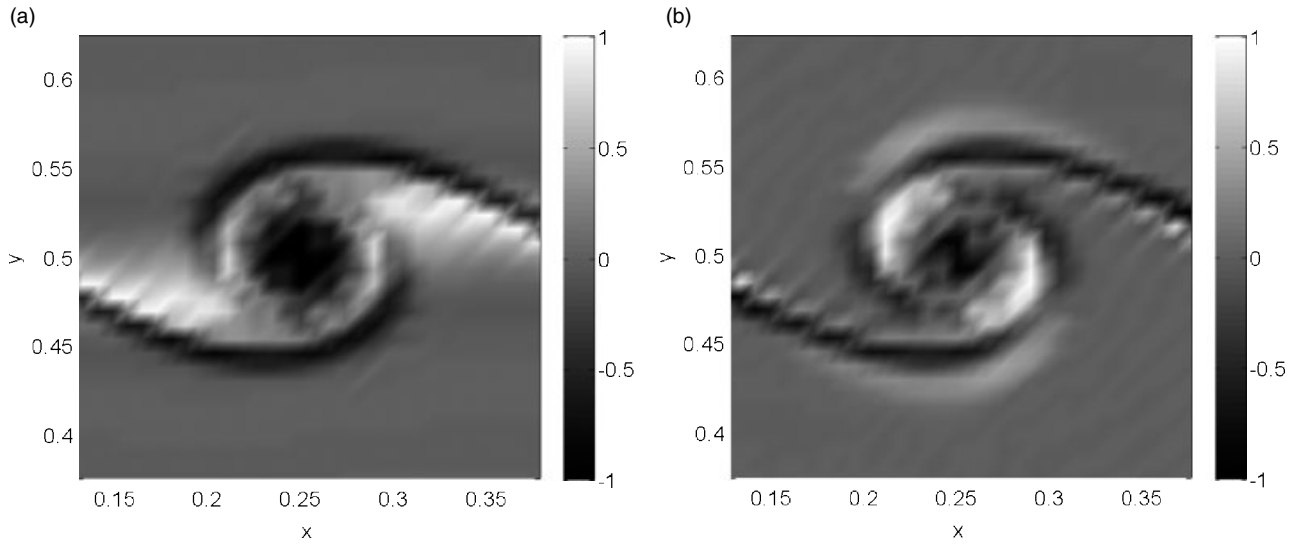

Figure 4. The cumulative truncation error for the Benchmark scheme (a) and the Utopia scheme (b) with the flux limiter for the vorticity strip test case at time 48.8 and on the 128^2 grid (zoomed in).

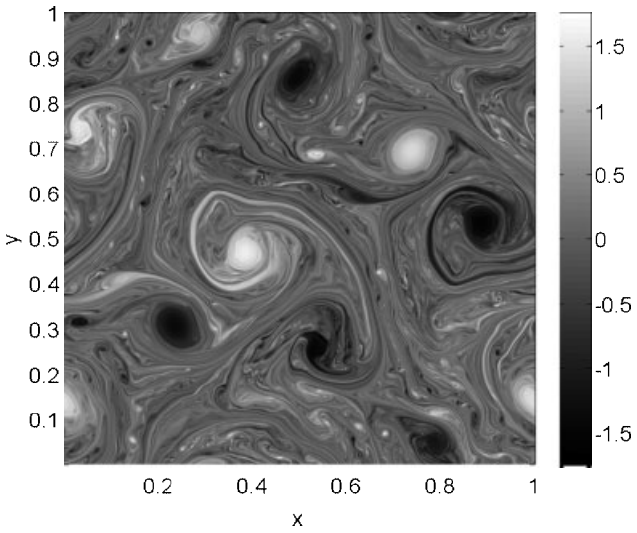

Figure 5. The high-resolution vorticity solution for the freely decaying turbulence test case at time 24.4.

is allowed to evolve for 73.2 time units on the HR grid. This new vorticity solution is then used as the initial condition for the freely decaying turbulence test ($t = 0$). The initial condition on the CR grid is obtained by averaging the $t = 0$ HR grid vorticity over each CR grid cell. A time step of $\Delta t = 5 \times 2^{-11}$ is used to ensure that the Courant number is less than 1 on the HR grid (and much less than 1 on the CR grids).

The HR reference solution at time $t = 24.4$ is shown in Figure 5. It shows a range of complex behaviour, including like-signed vortex pairs merging, opposite-signed vortex pairs propagating under mutual advection, vorticity strips being torn from large vortices and stretched, and vortex strips rolling up to form new vortices.

The left-hand panel of Figure 6 shows time series of the normalized l_2 vorticity error for five of the seven schemes listed in Table I with a CR grid resolution of 128^2. The Arakawa Jacobian without a simple subgrid model is unable to capture the subgrid term; the solution quickly becomes noisy and its l_2 error is significantly larger than that of any of the other schemes tested, and so is not shown on the plot. Each of the candidate ILES schemes has a smaller l_2 error than the Benchmark scheme: this is because the ILES schemes are modelling the effects of the subgrid terms better than the ∇^4 subgrid model. The results are similar for CR grids of resolution 32^2, 64^2 and 256^2.

Initially, for times t of order 1, there is a steep increase in the magnitude of the l_2 errors of all the numerical schemes. This is due to the schemes rapidly diffusing any grid-scale features that are present in the initial conditions. This corresponds to the sharp initial decrease of enstrophy (see Figure 8).

The right-hand plot of Figure 6 shows the normalized l_2 vorticity errors of the Lax–Wendroff flux limiter scheme in both advective form and flux form, the Utopia scheme and the SL scheme on the 128^2 grid. This provides a comparison between conservative and non-conservative schemes. The results show that the conservative schemes outperform the corresponding non-conservative schemes over long times. Therefore, conservation of vorticity appears to give a significant advantage to an ILES scheme for the BVE.

Figure 7 shows the total energy as a time series on the 128^2 grid for several schemes. The energy on CR scales of the HR reference solution is also shown to demonstrate that the energy on CR scales should increase slightly over time because of the upscale energy transfer from the subgrid scales. None of the CR schemes shown–either schemes considered for ILES or the Benchmark scheme with a simple subgrid model–is able to model this upscale energy transfer. Each of the schemes on the CR grid actually shows a significant decrease in the total energy: these schemes are necessarily diffusive to capture the diffusive effect of the subgrid term, but this diffusion leads to an unwanted dissipation of energy. Of the schemes shown, the Lax–Wendroff flux limiter scheme dissipates most energy, while the Utopia scheme dissipates least.

The total enstrophy for several schemes on the 128^2 grid is plotted as time series in Figure 8. The enstrophy on CR scales of the HR solution shows a steady decrease with time as its enstrophy cascades to smaller scales. The schemes shown are diffusive, either implicitly through their truncation error or through a simple subgrid model, and this dissipates the enstrophy. For each of the CR schemes, the enstrophy shows

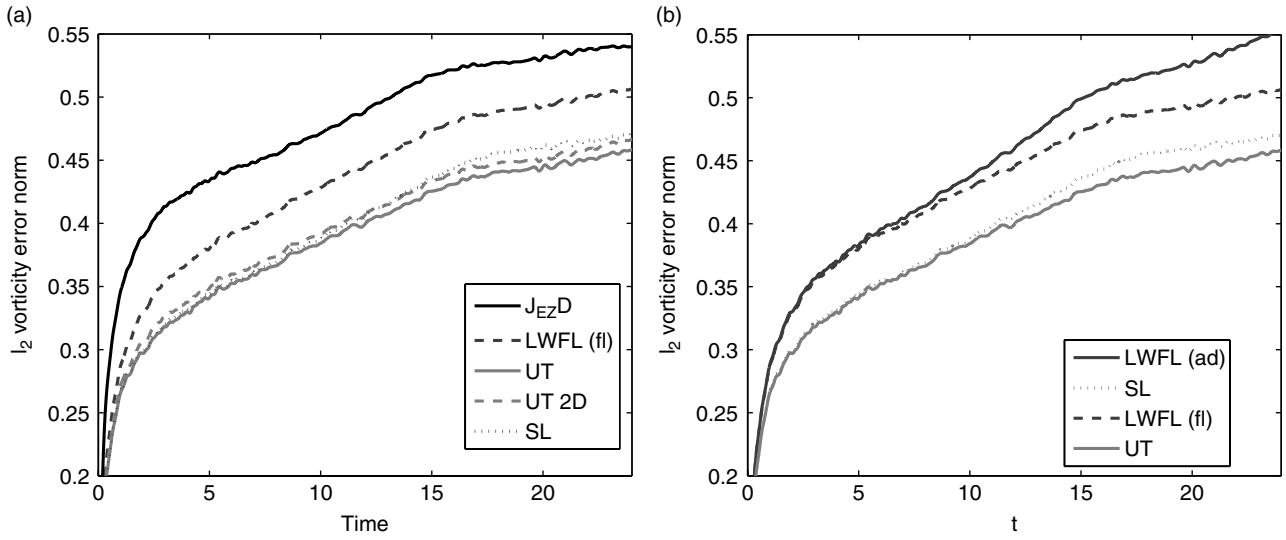

Figure 6. The normalized l_2 vorticity error norms for the freely decaying turbulence test case against time on the 128_2 grid (a). Also shown is a comparison of the normalized l_2 vorticity error norms of conservative and non-conservative schemes (b). The schemes shown are: the Benchmark scheme -$J_{EZ}D$, the Lax Wendroff flux limiter scheme -LWFL (in flux form -fl, and advective form -ad), the Utopia scheme -UT, the Utopia scheme with the two-dimensional flux limiter -UT 2D, and the semi-Lagrangian scheme -SL.

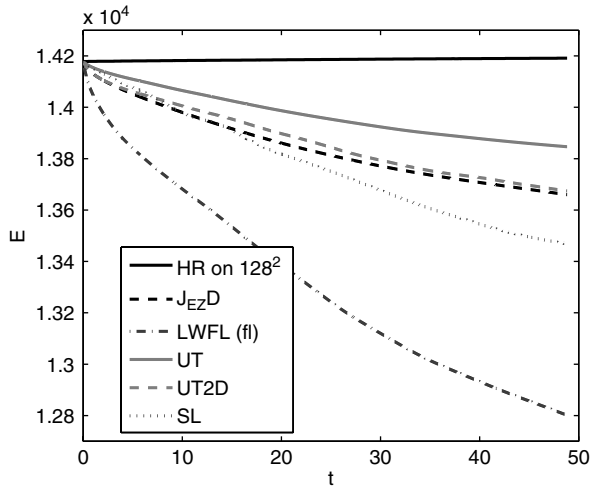

Figure 7. The total energy against time for the freely decaying turbulence test case on the 1282 grid. The scheme abbreviations are the same as those given in Figure 6.

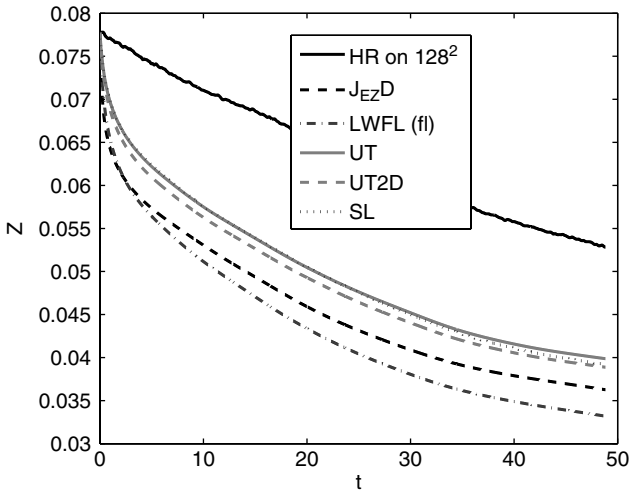

Figure 8. The total enstrophy against time for the freely decaying turbulence test case on the 1282 grid: note that the enstrophy for Utopia and SL is almost identical. The scheme abbreviations are the same as those given in Figure 6.

an initial rapid decrease followed by a longer-term steady decrease. The long-term rate of enstrophy loss is similar for the CR solutions and the CR-scale enstrophy of the HR solution. However, at any given time, the enstrophy of the CR solutions is significantly smaller than that at CR scales in the HR solution.

The Arakawa Jacobian conserves both energy and enstrophy, and is not shown in either Figure 7 or 8. Of all the schemes tested, the Arakawa Jacobian has the most similar energy time series to the CR-scale energy of the reference solution, but it cannot model the downscale enstrophy transfer; this leads to a build-up of grid scale noise and a highly inaccurate solution.

The l_2 error norms show that the Utopia scheme without a flux limiter is more accurate than the Utopia scheme with the flux limiter. This suggests that nonlinear diffusion is not a requirement of a successful ILES scheme for two-dimensional flow, provided the truncation errors are dominated by scale-selective dissipation. The Lax–Wendroff scheme does require the flux limiter to be successful for ILES; this is because the Lax–Wendroff scheme's leading truncation error is dispersive and is unable to capture the subgrid term. The Lax–Wendroff scheme without a flux limiter produces worse results than the Arakawa Jacobian for all test cases (not shown).

4.4. *Euler equations and potential vorticity equation*

The numerical tests were repeated using the velocity form of the Euler equations and the same methodology as used for the barotropic vorticity equation. The results for all of the test cases are very similar to those for the barotropic vorticity equation: the schemes considered for ILES are comparable in accuracy to the Benchmark scheme; the ILES schemes all capture the downscale enstrophy transfer, but none of them is able to model the upscale energy transfer. There is

one significant difference in the results between the velocity form and the vorticity form of the equations: the flux form of the Lax–Wendroff scheme with the van Leer limiter is not more accurate than the advective form for the velocity form of the equations. This suggests that the conservation of momentum is not as important as conservation of vorticity for implicit large eddy modelling of two-dimensional flow.

The numerical tests were also repeated for the quasi-geostrophic potential vorticity equation to investigate the effect of a finite Rossby radius on the application of ILES for two-dimensional flow. The freely decaying turbulence test case was used with (from (10)) $\lambda = 0.01$, 0.05, 0.1 and 0.25. The schemes considered for ILES were all more accurate than the Benchmark scheme regardless of the size of the Rossby radius. The subgrid model of the Benchmark scheme has to be tuned depending on the Rossby radius: the coefficient has to be reduced as the Rossby radius decreases. The ILES schemes, on the other hand, have no tunable parameters, yet all have a smaller l_2 vorticity error than the Benchmark scheme for each Rossby radius. As with the barotropic vorticity equation, none of the candidate ILES schemes or the Benchmark scheme could model the upscale energy transfer from the subgrid to the resolved scales, regardless of the Rossby radius.

5. Conclusions

The aim of this paper was to examine the validity of ILES for two-dimensional flow. Candidate numerical schemes considered for ILES were tested on a variety of test cases and compared with a Benchmark scheme (a second-order scheme (Arakawa, 1966) with scale-selective dissipation) for the BVE. The results showed that the ILES schemes were more accurate than the Benchmark scheme in terms of vorticity when comparing with a high-resolution reference solution. The cumulative effects of the subgrid term were compared with the cumulative effects of the truncation errors of the candidate numerical schemes. The candidate ILES schemes' truncation errors were a better match than the Benchmark scheme's truncation error when comparing with the subgrid term diagnosed using a high-resolution reference solution: this demonstrates that the ILES schemes are implicitly capturing the subgrid term better than a simple scale-selective dissipation. The ILES schemes were able to capture the diffusive effect of the subgrid term as vorticity was stretched below the grid scale (Type (i) behaviour), but they were unable to model the subgrid term when unresolved vorticity features interact with the resolved vorticity (Type (ii) behaviour). Similar results were found for the quasi-geostrophic potential vorticity equation for a range of Rossby radii.

The results from the numerical testing in vorticity form showed that the conservative flux form of the numerical schemes was measurably more accurate than the non-conservative advective form. Consistent with this, the Utopia scheme (which is in conservative flux form) was more accurate than the semi-Lagrangian scheme (which is not conservative). This suggests that the conservation of vorticity gives a significant advantage to an ILES scheme for the barotropic vorticity equation. Testing of the velocity form of the Euler equations showed that the scheme in flux form had no benefit, in terms of accuracy, compared with the scheme in advective form; this suggests that conservation of momentum is not essential to the success of ILES in two dimensions.

Another important question that stems from the three-dimensional ILES literature (see Grinstein and Fureby, 2006) is whether nonlinear diffusion, generated by, for example, a flux limiter, is required for ILES to be applied successfully to two-dimensional flow. To address this question a linear diffusive scheme (Utopia) was compared with a nonlinear diffusive scheme (Utopia with a two-dimensional limiter) for the BVE. The results for l_2 errors and for enstrophy time series show that the linearly diffusive scheme is at least as accurate (in some cases more accurate) as the nonlinearly diffusive scheme: this suggests that for two-dimensional flow nonlinear diffusion is not a requirement for an ILES scheme. (Nevertheless, a flux limiter might be desirable in contexts where it is essential to eliminate spurious amplification of extrema.)

Although the candidate ILES schemes and the Benchmark scheme could model the downscale enstrophy transfer, none of these schemes could model the upscale energy transfer from the subgrid to the resolved scales; in fact, the schemes dissipated energy. This work shows that ILES can be applied to two-dimensional flow with more accuracy than simple subgrid models, but that the ILES schemes cannot model the upscale energy transfer from the subgrid to the resolved scales.

The results presented here are likely to be applicable to two-dimensional and layerwise two-dimensional flows for which the near grid-scale dynamics is dominated by the nonlinear advection of vorticity or potential vorticity; this includes atmospheric flows on horizontal length scales larger than about 100 km, and shallow-water models in the appropriate parameter regime. However, atmospheric flows on horizontal scales smaller than about 100 km become increasingly dominated by gravity waves; our results are not intended to address the validity of ILES in this regime, or on even smaller scales where buoyant convection or three-dimensional turbulence can begin to become important.

Appendix

Decomposition of errors

Sagaut (2007) discusses three types of error that arise in the numerical solution of a nonlinear problem:

- *Projection error* occurs because a continuous field is represented by a finite number of degrees of freedom.
- *Discretization error* occurs because operators such as derivatives must be approximated, for example by finite differences.
- *Resolution error* occurs because the nonlinear terms in the numerical solution do not see all the scales of the nonlinear terms in the continuous problem.

Here we give explicit expressions for these three types of error for a spatial discretization of the barotropic vorticity equation, and relate these to the subgrid terms that our methodology diagnoses.

Write $\zeta^{(n)}$ for the numerical solution at some time in some grid cell. For a finite volume discretization it is natural

to interpret $\zeta^{(n)}$ as a grid cell average. We would like to write

$$\frac{\partial \zeta^{(n)}}{\partial t} + \overline{\nabla.(\mathcal{V}(\zeta)\zeta)} = e, \tag{34}$$

where ζ is the continuous solution for the vorticity, $\mathcal{V}$ is the operator defined by (4)–(6) that obtains the velocity vector from the vorticity, and overbar is a cell average filter of the form (20). Since the second term on the left-hand side is the exact nonlinear term, the right-hand side term e should be a measure of the error, i.e. the difference between $\partial\zeta^{(n)}/\partial t$ and $\partial\bar{\zeta}/\partial t$. However, the terms on the left-hand side of (34) live in different spaces: the first term is discrete whereas the second is continuous. We must therefore project the second term onto the discrete space in order to define the error:

$$\frac{\partial \zeta^{(n)}}{\partial t} + \mathcal{P}\left\{\overline{\nabla.(\mathcal{V}(\zeta)\zeta)}\right\} = e. \tag{35}$$

In this case a suitable projection operator is to sample the $\overline{\nabla.(\mathcal{V}(\zeta)\zeta)}$ field at the grid cell centres, which is equivalent to computing grid cell averages of $\nabla.(\mathcal{V}(\zeta)\zeta)$.

Now the numerical tendency $\partial\zeta^{(n)}/\partial t$ is computed as

$$\frac{\partial \zeta^{(n)}}{\partial t} + \nabla_h.(\mathcal{V}_h(\zeta^{(n)})\zeta^{(n)}) = 0, \tag{36}$$

where ∇_h and $\mathcal{V}_h$ are discrete approximations to ∇ and $\mathcal{V}$. Therefore

$$e = \mathcal{P}\left\{\overline{\nabla.(\mathcal{V}(\zeta)\zeta)}\right\} - \nabla_h.(\mathcal{V}_h(\zeta^{(n)})\zeta^{(n)}). \tag{37}$$

The error can be split into three components:

$$e = e_r + e_h + e_\pi \tag{38}$$

corresponding to the three error types discussed by Sagaut (2007)–resolution error:

$$e_r = \mathcal{P}\left\{\overline{\nabla.(\mathcal{V}(\zeta)\zeta)}\right\} - \mathcal{P}\left\{\overline{\nabla.(\mathcal{V}(\bar{\zeta})\bar{\zeta})}\right\}; \tag{39}$$

discretization error:

$$e_h = \mathcal{P}\left\{\overline{\nabla.(\mathcal{V}(\bar{\zeta})\bar{\zeta})}\right\} - \mathcal{P}\left\{\overline{\nabla_h.(\mathcal{V}_h(\bar{\zeta})\bar{\zeta})}\right\}; \tag{40}$$

and projection error:

$$e_\pi = \mathcal{P}\left\{\overline{\nabla_h.(\mathcal{V}_h(\bar{\zeta})\bar{\zeta})}\right\} - \nabla_h.(\mathcal{V}_h(\zeta^{(n)})\zeta^{(n)}). \tag{41}$$

Defining the subgrid terms using (17) and applying the projection operator shows that

$$\mathcal{P}\left\{\mathrm{SG}^*\right\} = -e_r. \tag{42}$$

A scheme will be a good ILES scheme provided $e \approx 0$, i.e. provided

$$e_h + e_\pi \approx -e_r = \mathcal{P}\left\{\mathrm{SG}^*\right\}. \tag{43}$$

That is, the discretization plus projection errors must match the projection of the subgrid term.

Acknowledgements

This paper is based on part of the PhD thesis of the first author, whose study at the University of Exeter was sponsored by Great Western Research and the Met Office. We would like to thank two anonymous reviewers for their helpful comments.

References

Arakawa A. 1966. Computational design for long-term numerical integration of the equations of fluid motion: two-dimensional incompressible flow. Part I. *J. Comput. Phys.* **1**: 119–143.

Berloff PS. 2005. Random-forcing model of the mesoscale ocean eddies. *J. Fluid Mech.* **529**: 71–95.

Brown AR, MacVean MK, Mason PJ. 2000. The effects of numerical dissipation in large eddy simulations. *J. Atmos. Sci.* **57**: 3337–3348.

Fulton SR, Ciesielski PE, Schubert WH. 1986. Multigrid methods for elliptic problems: a review. *Mon. Weather Rev.* **114**: 943–959.

Gill AE. 1982. *Atmosphere–Ocean Dynamics*. Academic Press: New York.

Grinstein FF, Fureby C. 2006. Recent progress on flux-limiting based implicit large eddy simulation. In *European Conference on Computational Fluid Dynamics, ECCOMAS CFD 2006*.

Grinstein FF, Margolin LG, Rider WJ. 2007a. A rationale for implicit LES. In *Implicit Large-Eddy Simulation*, Grinstein FF, Margolin LG, Rider WJ (eds). Cambridge University Press: Cambridge, UK; 39–58.

Grinstein FF, Margolin LG, Rider WJ. 2007b. *Implicit Large Eddy Simulation*. Cambridge University Press: Cambridge, UK.

Hermanson L, Hoskins BJ, Palmer TN. 2009. A comparative method to evaluate and validate stochastic parametrizations. *Q. J. R. Meteorol. Soc.* **135**: 1095–1103.

Jablonowski C, Williamson DL. 2011. The pros and cons of diffusion, filters and fixers in atmospheric general circulation models. In *Numerical Techniques for Global Atmospheric Models*, Lauritzen PH, Jablonowski C, Taylor MA, Nair RD (eds). Springer: Berlin; 389–504.

Lauritzen PH, Nair RD, Ullrich PA. 2010. A conservative semi-Lagrangian multi-tracer transport scheme (CSLAM) on the cubed-sphere grid. *J. Comput. Phys.* **229**: 1401–1424.

Leonard A. 1975. Energy cascade in large-eddy simulations of turbulent fluid flows. *Adv. Geophys.* **18**(i): 237–248.

Leonard BP, MacVean MK, Lock AP. 1993. *Positivity-preserving numerical schemes for multidimensional advection*. NASA Technical Memorandum 106055.

Lin SJ. 2004. A 'vertically Lagrangian' finite-volume dynamical core for global models. *Mon. Weather Rev.* **132**: 2293–2307.

Margolin LG, Rider WJ. 2002. A rationale for implicit turbulence modeling. *Int. J. Numer. Meth. Fl.* **39**: 821–841.

Margolin LG, Rider WJ. 2007. Numerical regularization: the numerical analysis of implicit subgrid models. In *Implicit Large-Eddy Simulation*, Grinstein FF, Margolin LG, Rider WJ (eds). Cambridge University Press: Cambridge, UK; 195–221.

Sagaut P. 2001. *Large Eddy Simulation for Incompressible Flows*. Springer: Berlin.

Sagaut P. 2007. Subgrid-scale modeling: issues and approaches. In *Implicit Large-Eddy Simulation*, Grinstein FF, Margolin LG, Rider WJ (eds). Cambridge University Press: Cambridge, UK; 61–93.

Staniforth A, Côté J. 1991. Semi-Lagrangian integration schemes for atmospheric models: a review. *Mon. Weather Rev.* **119**: 2206–2223.

Thuburn J. 1996. Multidimensional flux-limited advection schemes. *J. Comput. Phys.* **123**: 74–83.

Ullrich PA, Jablonowksi C, van Leer B. 2010. High-order finite-volume methods for the shallow-water equations on the sphere. *J. Comput. Phys.* **229**: 6104–6134.

van Leer B. 1974. Towards the ultimate conservative difference scheme. II. Monotonicity and conservation combined in a second order scheme. *J. Comput. Phys.* **14**: 361–370.

Williamson DL. 2007. The evolution of dynamical cores for global atmospheric models. *J. Meteorol. Soc. Jpn.* **85B**: 241–269.

Zerroukat M, Wood N, Staniforth A. 2002. SLICE: a semi-Lagrangian inherently conserving and efficient scheme for transport problems. *Q. J. R. Meteorol. Soc.* **128**: 2801–2820.